Sequential multiphoton strategy for semiconductor-based terahertz detectors

Fabrizio Castellano,[a] Rita C. Iotti, and Fausto Rossi
Dipartimento di Fisica, Politecnico di Torino, Corso Duca degli Abruzzi 24, 10129 Torino, Italy

(Received 17 June 2008; accepted 3 November 2008; published online 17 December 2008)

A semiconductor-based terahertz-detector strategy, exploiting a bound-to-bound-to-continuum architecture, is presented and investigated. In particular, a ladder of equidistant energy levels is employed, whose step is tuned to the desired detection frequency and allows for sequential multiphoton absorption. Our theoretical analysis demonstrates that the proposed multisubband scheme could represent a promising alternative to conventional quantum-well infrared photodetectors in the terahertz spectral region. © *2008 American Institute of Physics*.
[DOI: 10.1063/1.3043577]

I. INTRODUCTION

The recent development of reliable far-infrared (far-IR) semiconductor-based laser sources, such as the quantum-cascade (QC) laser,[1,2] together with the potential applications in imaging, communication, and medicine, identifies terahertz radiation detection as a crucial technological milestone. To this end, many approaches have been proposed in the past years, which aim at accessing the 1–10 THz region of the electromagnetic spectrum. Currently proposed solutions encompass a variety of different approaches, each with its own peculiar characteristics.

From the electronics world, field effect transistors are extending their operation frequency into the subterahertz and terahertz region exploiting plasmon resonance effects.[3–5] On the other hand, optoelectronic techniques benefiting from electro-optical properties of $LiTaO_3$, $LiNbO_3$, and ZnTe crystals were proposed.[6,7]

Semiconductor heterostructures also play a fundamental role in this field, QC structures[8,9] as well as quantum-well infrared photodetectors (QWIPs) (Ref. 10) being among the most promising directions. Concerning the latter, radiation detection via conventional QWIP designs resorts on direct bound-to-continuum electronic transitions, which allowed achieving remarkable levels of performance in the mid-IR range. Recently, the use of multilevel architectures, opening up to bound-to-bound electronic transitions, has been proposed and studied, focusing both on their intrinsic nonlinear character and on their wide-band absorption spectra. While the latter feature allows for multicolor[11] or wideband detection,[12–15] second-order nonlinearities of two-level systems have been studied and experimentally demonstrated with the idea of using the devices for second-order autocorrelation measurements.[16–19]

The extension of the conventional, bound-to-continuum, QWIP principle into the far-IR range is not straightforward. In particular, one of the main issues in terahertz-operating devices is the huge dark current value that causes the background limited infrared photodetection temperature (T_{blip}) to be in the range of 10–15 K,[20,21] that is, much lower than that of state-of-the-art mid-IR QWIPs. In a previous work,[22] we addressed the advantages of the application of multilevel architecture in terahertz QWIP designs and concluded that a bound-to-bound-to-continuum scheme may efficiently face the above-mentioned dark current issue. More recently,[23] we have analyzed the performances of such novel architecture, focusing on the characteristic figure of merit T_{blip}. Our results suggest the possibility to achieve a consistent improvement of the operation temperature of terahertz QWIPs by means of our proposed multilevel design. In the present article, our findings are further discussed and the theoretical model on which our calculations are based is explained in more detail.

II. PHYSICAL SYSTEMS AND MODELING STRATEGY

Our prototypical device consists of an infinitely periodic semiconductor-based heterostructure supporting, within each period, a set of equally spaced bound states. The physical system we are considering is therefore an electron gas within a periodic nanostructure and in the presence of external electromagnetic fields. The corresponding Hamiltonian can be schematically written as

$$\hat{H} = \hat{H}^{\circ} + \hat{H}' . \tag{1}$$

The first term in Eq. (1),

$$\hat{H}^{\circ} = \hat{H}^{\circ}_{e} + \hat{H}^{\circ}_{qp} = \sum_{\alpha} \epsilon_{\alpha} \hat{c}^{\dagger}_{\alpha} \hat{c}_{\alpha} + \sum_{\lambda \mathbf{q}} \epsilon_{\lambda \mathbf{q}} \hat{b}^{\dagger}_{\lambda \mathbf{q}} \hat{b}_{\lambda \mathbf{q}} \tag{2}$$

is the sum of the free-carrier ($\hat{H}^{\circ}_{e}$) and free-quasiparticle ($\hat{H}^{\circ}_{qp}$) Hamiltonians, where the fermionic operator $\hat{c}^{\dagger}_{\alpha}$ ($\hat{c}_{\alpha}$) denotes creation (destruction) of a carrier in the single particle state α, with energy ϵ_{α}, while the bosonic operator $\hat{b}^{\dagger}_{\lambda \mathbf{q}}$ ($\hat{b}_{\lambda \mathbf{q}}$) denotes creation (destruction) of a quasiparticle excitation of type λ (phonons, photons, plasmons, etc.) with wavevector $\mathbf{q}$.

The Hamiltonian $\hat{H}'$ in Eq. (1) is the sum of all possible interaction terms between electrons and quasiparticles. Since the aim of the present paper is to provide a focus on the electron-photon interaction dynamics, the latter will be

[a]Electronic mail: fabrizio.castellano@polito.it.

treated in a fully microscopic scheme, in terms of the Fermi's golden rule. Conversely, all the other carrier-quasiparticle interactions will be described within a phenomenological electronic mean-lifetime picture, providing effective scattering probabilites that guarantee the proper thermalization of the electron population in the absence of external electromagnetic fields.

A. Band structure calculation

The single-particle Hamiltonian $\hat{H}_e^\circ$ describes the noninteracting carrier system within the effective three-dimensional potential profile of our quantum device. The generic label α adopted in Eq. (2) denotes, in general, a suitable set of discrete and/or continuous quantum numbers; for the case of quasi-two-dimensional semiconductor heterostructures, as the ones considered in this paper, the latter includes a partially discrete index along the so-called growth direction. In particular, since our prototypical design is made up of a sequence of identical units, the potential term consists, in the envelope-function formalism, of a periodic one-dimensional (1D) profile.

For a device grown along the z-direction and homogeneous as far as the in-plane (x,y) dynamics is concerned, the following factorization of the electron wave function may then be assumed:

$$\Psi_{bk_z\mathbf{k}_p}(\mathbf{r}) = \psi_{b,k_z}(z)\phi_{\mathbf{k}_p}(x,y), \tag{3}$$

where $\mathbf{k}_p$ and k_z are the in-plane and along-z components of the electron wavevector $\mathbf{k}$, respectively, and b is the label numbering the various discrete subbands in which the conduction band is split because of the 1D quantum confinement potential.

While parabolic bands are considered for the in-plane dispersion, and $\phi_{\mathbf{k}_p}(x,y)$ is the corresponding plane wave, the band structure along the growth direction is computed from the 1D Schrödinger equation for the given potential profile. Moreover, due to the typically low doping levels in this kind of devices, charge-density effects on the potential profile may safely be neglected and no Schrödinger–Poisson coupling is included in our modeling.

The Schrödinger equation projected along the z direction is solved by means of a plane-wave expansion, as described in Ref. 24. The following basis functions may then be adopted

$$\chi_{n,k_z}(z) = \frac{1}{\sqrt{L_z}} e^{i(G_n+k_z)z}, \tag{4}$$

where n is an integer running from $-N$ to N, L_z is the period of the 1D potential (i.e., the supercell width), and $G_n = 2\pi n/L_z$ and k_z $(-\pi/L_z < k_z < \pi/L_z)$ are the reciprocal lattice vector and the quasimomentum in the first Brillouin zone, respectively. The basis functions are normalized, as usual, over the supercell

$$\int_{-L_z/2}^{L_z/2} \chi^*_{n,k_z}\chi_{m,k_z}dz = \delta_{nm}. \tag{5}$$

In a reduced-zone scheme we can express the along-z wave function of an electron in subband b and momentum k_z as

$$\psi_{b,k_z}(z) = \sqrt{\frac{L_z}{2\pi}} \sum_{n=-N}^{N} c_{b,n,k_z}\chi_{n,k_z}(z). \tag{6}$$

The series expansion in Eq. (6) allows us to convert the stationary Schrödinger equation into a discrete eigenvalue problem. The solution of such problem consists of a set of $2N+1$ energy eigenvalues ϵ_{b,k_z}, each representing the allowed energy level for an electron in subband b with wavevector k_z. The components c_{b,n,k_z} represent the spectrum of the wave function in the plane wave basis set. The plane-wave-like normalization of the wave functions $\Psi_{b,k_z,\mathbf{k}_p}$,

$$\langle \Psi_{bk_z'\mathbf{k}_p'} | \Psi_{bk_z\mathbf{k}_p} \rangle = \int \Psi^*_{bk_z'\mathbf{k}_p'}(\mathbf{r})\Psi_{bk_z\mathbf{k}_p}(\mathbf{r})d\mathbf{r} = \delta(\mathbf{k}-\mathbf{k}'), \tag{7}$$

is guaranteed by the form (4) of the basis functions and is consistent with the fact that the structure is assumed to be infinite along z.

B. Potential profile

The quantum design of our semiconductor device should satisfy several requirements. First of all, the main constrain is to have equally spaced bound levels. Second, we want to be able to control the number of such levels and their spacing, too.

When speaking of equally spaced levels, the first solution would seem to be that of a parabolic potential profile. The implementation of the latter, however, besides nontrivial growth issues, poses more fundamental problems: in order to have carrier transport we need a continuum and thus the parabolic potential must be truncated at some point. Such a truncated parabola would not support equally spaced levels anymore. We therefore decide to use multi-quantum-well strategies for our QWIP basic period.

Single quantum wells are used to produce the single bound level providing the bound-to-continuum transition exploited in conventional QWIPs. Two energetically equal transitions can still be obtained with a single QW of proper geometry. The tuning of the separations of three bound levels cannot be achieved with a potential having only two free parameters (width and depth) and thus we have to switch to more complex structures.

The nested QW structures—shown in Fig. 1—turn out to be convenient choices. The introduction of additional geometrical parameters to the standard QW design allow us to control the number and position of the desired number of energy levels. A detailed description of the method used to determine the potential profiles is given in Appendix A.

Figure 1 shows the supercells of our prototypical structures, which are to be infinitely replicated along the growth direction. The use of many repetitions of the basic unit is indeed the strategy exploited in this kind of unipolar devices to optimize detection efficiency. Finite-size (i.e., boundary

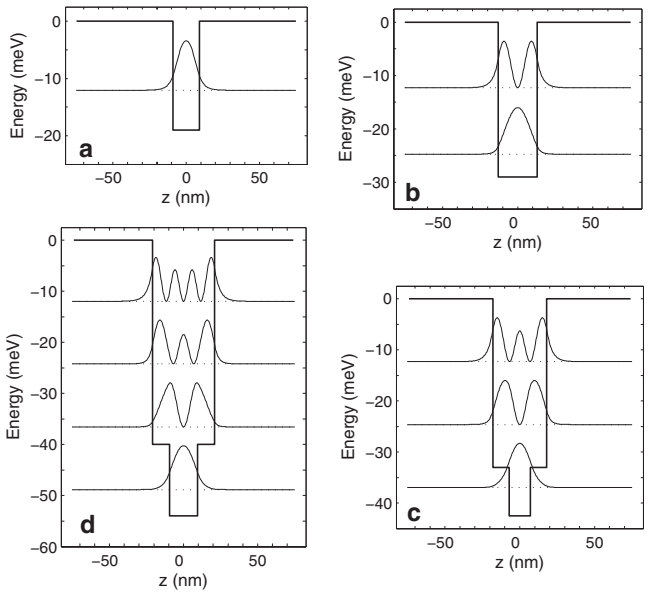

FIG. 1. Potential profiles along the growth direction of our prototypical devices, designed to operate at 3 THz, with a number of bound states varying from one (a) to four (d). The proposed symmetric nested-quantum-well structure in (c) and (d) provides additional geometric parameters, with respect to the single QW design, which can be varied to tune the energy level separation.

and contact) effects are therefore of minor importance. Moreover, due to the low doping values, in-plane quantum confinement effects are negligible, too.

C. Transport model

The transport model we employ to describe the electron dynamics in our unipolar device is based on the Boltzmann transport equation describing the distribution of electrons in the device conduction band. Its general form for the case of N subbands is the following:

$$\frac{\partial f_b(\mathbf{k})}{\partial t} = \frac{e}{\hbar}\mathbf{F}\cdot\nabla f_b(\mathbf{k}) + \sum_{b'=1}^{N}\int [P_{bb'}(\mathbf{k},\mathbf{k}')f_{b'}(\mathbf{k}') - P_{b'b}(\mathbf{k}',\mathbf{k})f_b(\mathbf{k})]d\mathbf{k}', \tag{8}$$

where $f_b(\mathbf{k})$ is the single-particle distribution function of electrons in a state with wavevector $\mathbf{k}$ in subband b, $P_{b'b}(\mathbf{k}',\mathbf{k})\mathrm{d}\mathbf{k}'$ is the probability per unit time that a scattering event bringing an electron from a state in band b and wavevector $\mathbf{k}$ to a state in band b' and wavevector $\mathbf{k}'$ occurs, and $\mathbf{F}$ is the external electric field providing the electron drift. $\mathbf{F}$ may in general be oriented in any direction; in this paper, we will limit our discussion to biases applied only along the growth axis. The knowledge of $f_b(\mathbf{k})$ allows us to evaluate the current density across the device, $\mathcal{J}$, as follows

$$\langle \mathcal{J} \rangle = \frac{e}{(2\pi)^3\hbar}\sum_b \int \nabla E_b(\mathbf{k}) f_b(\mathbf{k}) d\mathbf{k}, \tag{9}$$

provided that the distribution function is normalized as

$$\frac{1}{(2\pi)^3}\sum_b \int f_b(\mathbf{k})d\mathbf{k} = N_e, \tag{10}$$

where $E_b(\mathbf{k})$ is the miniband dispersion and N_e is the number of electrons per unit volume in the device.

Being interested in the steady-state behavior of our device, we solve the homogeneous equation obtained from Eq. (8) when the time derivative is set equal to zero

$$\frac{e}{\hbar}\mathbf{F}\cdot\nabla f_b(\mathbf{k}) + \sum_{b'=1}^{N}\int [P_{bb'}(\mathbf{k},\mathbf{k}')f_{b'}(\mathbf{k}') - P_{b'b}(\mathbf{k}',\mathbf{k})f_b(\mathbf{k})]d\mathbf{k}' = 0. \tag{11}$$

The latter equation is solved employing a finite difference strategy as described in Appendix B. The various scattering mechanisms affecting the electron dynamics are included into the global probabilities $P_{b'b}(\mathbf{k}',\mathbf{k})$ and may be separated into the following contributions:

$$P_{b'b}(\mathbf{k}',\mathbf{k}) = P^{\mathrm{opt}}_{b'b}(\mathbf{k}',\mathbf{k}) + P^{\mathrm{th}}_{b'b}(\mathbf{k}',\mathbf{k}), \tag{12}$$

where $P^{\mathrm{opt}}_{b'b}(\mathbf{k}',\mathbf{k})$ is the electron-photon interaction part and $P^{\mathrm{th}}_{b'b}(\mathbf{k}',\mathbf{k})$ accounts for all thermalization processes.

D. Nonoptical scattering model

To keep the model as simple as possible, yet without spoiling the proper description of the main physical issues, all nonoptical scattering processes are accounted for by means of a phenomenological mean lifetime τ, which acts as a global fitting parameter. Let us introduce a thermal transition probability density $P^{\mathrm{th}}_{bb'}(\mathbf{k},\mathbf{k}')$ such that the mean lifetime $\tau_{b\mathbf{k}}$ of an electron in band b with wavevector $\mathbf{k}$ is given by

$$\frac{1}{\tau_{b\mathbf{k}}} = \sum_{b'}\int P^{\mathrm{th}}_{b'b}(\mathbf{k}',\mathbf{k})d\mathbf{k}'. \tag{13}$$

The mean lifetime of the electrons τ is then defined in terms of the distribution function $f_b(\mathbf{k})$ as

$$\frac{1}{\tau} = \frac{1}{(2\pi)^3 N_e}\sum_b \int \frac{f_b(\mathbf{k})}{\tau_{b\mathbf{k}}}d\mathbf{k} = \frac{1}{(2\pi)^3 N_e}\sum_{bb'}\int\int f_b(\mathbf{k})P^{\mathrm{th}}_{b'b}(\mathbf{k}',\mathbf{k})d\mathbf{k}'d\mathbf{k}. \tag{14}$$

The latter can be used to compute the P^{th} probabilities once τ has been fixed and a functional form for P^{th} has been set. However, the definition of τ given in Eq. (14) implies the knowledge of the single-particle distribution function, which is obtained from Eq. (11), which in turn requires P^{th} to be determined. To break this loop we choose to drop the strict physical interpretation of τ as the actual mean lifetime of electrons and simply use it as a measure of the strength of thermalization mechanisms. In this picture we can perform the mean in Eq. (14) using a distribution function of our choice and convenience, bearing in mind that this will not affect our conclusions. We thus define τ as

$$\frac{1}{\tau} = \frac{1}{(2\pi)^3 N_e} \sum_{bb'} \int \int P^{\text{th}}_{b'b}(\mathbf{k}',\mathbf{k}) d\mathbf{k}' d\mathbf{k}. \tag{15}$$

To evaluate the integral in Eq. (15), we have to choose a functional form for P^{th} containing a free parameter suitable for normalization. Since P^{th} must account for all thermalization mechanisms, its form must ensure that in the absence of any external excitation (i.e., no bias, no light) the system exhibits a thermal distribution function, that is, a distribution function such that

$$\frac{f_b(\mathbf{k})}{f_{b'}(\mathbf{k}')} = e^{-[E_b(\mathbf{k})-E_{b'}(\mathbf{k}')]/k_B T}. \tag{16}$$

At equilibrium we know from the detailed-balance principle that

$$\frac{f_b(\mathbf{k})}{f_{b'}(\mathbf{k}')} = \frac{P^{\text{th}}_{bb'}(\mathbf{k},\mathbf{k}')}{P^{\text{th}}_{b'b}(\mathbf{k}',\mathbf{k})} \tag{17}$$

the simpler way to fulfill this requirement is to impose

$$\begin{aligned} P^{\text{th}}_{b'\mathbf{k}',b\mathbf{k}} &= P_0 \mathcal{P}_{b'b}(\mathbf{k}'\mathbf{k}) \\ &= P_0 \begin{cases} 1 & \text{if } E_b(\mathbf{k}) > E_{b'}(\mathbf{k}') \\ e^{-[E_{b'}(\mathbf{k}')-E_b(\mathbf{k})]/k_B T} & \text{if } E_b(\mathbf{k}) < E_{b'}(\mathbf{k}'), \end{cases} \end{aligned} \tag{18}$$

where P_0 is a normalization constant that can be computed in terms of τ as follows

$$\frac{1}{P_0} = \frac{\tau}{(2\pi)^3 N_e} \sum_{bb'} \int \mathcal{P}_{b'b}(\mathbf{k}',\mathbf{k}) d\mathbf{k}' d\mathbf{k}. \tag{19}$$

The strategy is therefore to first assume a value for τ and then use the latter to compute P_0. This completely determines the probabilities P^{th} that appear in Eq. (12) and allows us to solve Eq. (11).

Actually the definition of P_0 would not be of any importance if thermal scattering was the only scattering process but, since we want to investigate its competition/interplay with carrier-photon interaction, P_0 (and consequently τ) is the parameter that allows us to adjust the relative strength of the two mechanisms.

E. Electron-photon interaction

To evaluate the T_{blip} of our prototypical device, we have to properly describe the interaction between the electron population and the radiation field of an external blackbody source.

The second-quantization electric- and magnetic-field operators for a plane electromagnetic wave with wavevector $\mathbf{q}$ have the form

$$\hat{\mathbf{E}}_\mathbf{q} = \frac{|\mathbf{E}_\mathbf{q}|}{\sqrt{2}} \mathbf{e}_\mathbf{q} (e^{i(\omega_\mathbf{q} t - \mathbf{q}\cdot\mathbf{r})} \hat{a}_\mathbf{q} + e^{-i(\omega_\mathbf{q} t - \mathbf{q}\cdot\mathbf{r})} \hat{a}^\dagger_\mathbf{q}), \tag{20}$$

$$\hat{\mathbf{B}}_\mathbf{q} = \frac{|\mathbf{B}_\mathbf{q}|}{\sqrt{2}} \mathbf{b}_\mathbf{q} (e^{i(\omega_\mathbf{q} t - \mathbf{q}\cdot\mathbf{r})} \hat{a}_\mathbf{q} + e^{-i(\omega_\mathbf{q} t - \mathbf{q}\cdot\mathbf{r})} \hat{a}^\dagger_\mathbf{q}), \tag{21}$$

or alternatively

$$\hat{\mathbf{E}}_\mathbf{q} = \sqrt{\frac{\hbar\omega_\mathbf{q}}{2\epsilon\mathcal{V}}} \mathbf{e}_\mathbf{q} (e^{i(\omega_\mathbf{q} t - \mathbf{q}\cdot\mathbf{r})} \hat{a}_\mathbf{q} + e^{-i(\omega_\mathbf{q} t - \mathbf{q}\cdot\mathbf{r})} \hat{a}^\dagger_\mathbf{q}), \tag{22}$$

$$\hat{\mathbf{B}}_\mathbf{q} = \sqrt{\frac{\hbar\omega_\mathbf{q}\mu}{2\mathcal{V}}} \mathbf{b}_\mathbf{q} (e^{i(\omega_\mathbf{q} t - \mathbf{q}\cdot\mathbf{r})} \hat{a}_\mathbf{q} + e^{-i(\omega_\mathbf{q} t - \mathbf{q}\cdot\mathbf{r})} \hat{a}^\dagger_\mathbf{q}), \tag{23}$$

where $\mathbf{E}_\mathbf{q}$ and $\mathbf{B}_\mathbf{q}$ are the classical electric and magnetic fields, $\omega_\mathbf{q}$ is the dispersion relation of the medium, ε is the dielectric constant, μ the magnetic permittivity, $\mathcal{V}$ is the device volume, $\mathbf{e}_\mathbf{q}$ and $\mathbf{b}_\mathbf{q}$ are the polarization unit vectors such that $\mathbf{e}_\mathbf{q}\cdot\mathbf{q} = \mathbf{b}_\mathbf{q}\cdot\mathbf{q} = \mathbf{e}_\mathbf{q}\cdot\mathbf{b}_\mathbf{q} = 0$, and $\hat{a}_\mathbf{q}$ and $\hat{a}^\dagger_\mathbf{q}$ are destruction and creation operators, respectively, for a photon of wavevector $\mathbf{q}$.

The expressions above allow us to write the electric and magnetic field operators in the case of a linear superposition of plane waves as

$$\hat{\mathbf{E}} = \sum_\mathbf{q} \hat{\mathbf{E}}_\mathbf{q}, \tag{24}$$

$$\hat{\mathbf{B}} = \sum_\mathbf{q} \hat{\mathbf{B}}_\mathbf{q}. \tag{25}$$

With the latter definition, we can easily recover the usual expression for the second quantization Hamiltonian of a population of photons in terms of the energy density operator $\hat{U}(\mathbf{r})$,

$$\begin{aligned} \hat{H}^\circ_{\text{ph}} = \int_\mathcal{V} \hat{U}(\mathbf{r}) d\mathbf{r} = \int_\mathcal{V} \sum_\mathbf{q} \Bigg(\frac{1}{2}\varepsilon \hat{\mathbf{E}}_\mathbf{q}\cdot\hat{\mathbf{E}}^\dagger_\mathbf{q} + \frac{1}{2\mu}\hat{\mathbf{B}}_\mathbf{q}\cdot\hat{\mathbf{B}}^\dagger_\mathbf{q} \\ - \frac{\hbar\omega_\mathbf{q}}{2\mathcal{V}} \Bigg) d\mathbf{r} = \sum_\mathbf{q} \hbar\omega_\mathbf{q} \hat{a}^\dagger_\mathbf{q} \hat{a}_\mathbf{q}. \end{aligned} \tag{26}$$

In this picture, the classical energy density, $U(\mathbf{r}) = \frac{1}{2}\varepsilon\Sigma_\mathbf{q} E^2_\mathbf{q} + 1/2\mu\Sigma_\mathbf{q} B^2_\mathbf{q}$, refers to the zero-point energy density $\hbar\omega_\mathbf{q}/2\mathcal{V}$ of the electromagnetic field in a cavity of volume $\mathcal{V}$.

Given the electric field operator $\hat{\mathbf{E}}$, we can define the vector potential operator $\hat{\mathbf{A}}$ as

$$\hat{\mathbf{A}} = \sum_\mathbf{q} \hat{\mathbf{A}}_\mathbf{q} = \sum_\mathbf{q} \frac{1}{\sqrt{2}} (\mathbf{A}_\mathbf{q} \hat{a}_\mathbf{q} + \mathbf{A}^*_\mathbf{q} \hat{a}^\dagger_\mathbf{q}) = \sum_\mathbf{q} \frac{\hat{\mathbf{E}}_\mathbf{q}}{i\omega_\mathbf{q}}, \tag{27}$$

where $\mathbf{A}_\mathbf{q}$ is the classical vector potential, having implicitly assumed a gauge where $\mathbf{E} = \partial\mathbf{A}/\partial t$.

In a second-quantization picture, the electron-photon interaction Hamiltonian operator

$$\hat{H}^{\text{opt}} = -i\hbar\frac{e}{m}\nabla\cdot\hat{\mathbf{A}} = -\frac{i\hbar e}{m\sqrt{2}} \sum_\mathbf{q} (\nabla\cdot\mathbf{A}_\mathbf{q}\hat{a}_\mathbf{q} + \nabla\cdot\mathbf{A}^*_\mathbf{q}\hat{a}^\dagger_\mathbf{q}) \tag{28}$$

can be written as

$$\hat{H}^{\text{opt}} = \sum_{\alpha\alpha'\mathbf{q}} [g_{\alpha\alpha'\mathbf{q}} \hat{c}^{\dagger}_{\alpha} \hat{a}_{\mathbf{q}} \hat{c}_{\alpha'} + g^{*}_{\alpha\alpha'\mathbf{q}} \hat{c}^{\dagger}_{\alpha'} \hat{a}^{\dagger}_{\mathbf{q}} \hat{c}_{\alpha}]. \tag{29}$$

Here, the first (second) contribution describes a process in which an electron performs a transition between the two single-particle states $\alpha=(b,k_z,\mathbf{k}_p)$ and $\alpha'=(b',k'_z,\mathbf{k}'_p)$ absorbing (emitting) a photon; this mechanism has a coupling constant g, which is expressed as

$$g_{\alpha\alpha'\mathbf{q}} = -\frac{i\hbar e}{m\sqrt{2}} \int d\mathbf{r} \Psi^{*}_{\alpha} (\nabla \cdot \mathbf{A}_{\mathbf{q}}) \Psi_{\alpha'}. \tag{30}$$

The evaluation of $g_{\alpha\alpha'\mathbf{q}}$ from Eq. (30) can be carried out in terms of the plane wave expansion of Ψ_{α} given in Eqs. (3) and (6)

$$g_{bk_z\mathbf{k}_p,b'k'_z\mathbf{k}'_p,\mathbf{q}} = \frac{\hbar e}{m\sqrt{2}} \delta(\mathbf{k}+\mathbf{q}-\mathbf{k}') \times \sum_{n} c^{*}_{b'nk'_z} c_{bnk_z} [A_{z,\mathbf{q}}(q_z + G_n + k_z) + \mathbf{A}_{p,\mathbf{q}} \cdot \mathbf{k}_p], \tag{31}$$

where $A_{z,\mathbf{q}}$ and $\mathbf{A}_{p,\mathbf{q}}$ are the along-z and in-plane components of the vector potential, respectively.

Equation (31) may be simplified in several ways. First of all, the usual dipole approximation allows neglecting the photon momentum $\mathbf{q}$ with respect to the electron momentum $\mathbf{k}$.

Since we have assumed a parabolic in-plane dispersion, and since we expect electrons to have a quasithermal distribution, then the great majority of them will occupy states close to the subband bottom ($k_p \approx 0$). On the other hand, the minibands along k_z are either flat or slightly dispersive, that is, much narrower that the related subbands. Therefore we may assume that, for the majority of the electrons, $k_p \ll (G_n + k_z)$.

This leads to the following simplified expression for the coupling constant:

$$g_{\alpha\alpha',\mathbf{q}} = \frac{\hbar e}{m\sqrt{2}} \delta(\mathbf{k}_{\alpha} - \mathbf{k}_{\alpha'}) |\mathbf{A}_{\mathbf{q}}| \cos\varphi_{\mathbf{q}} \sum_{n} c^{*}_{b'nk'_z} c_{bnk_z} (G_n + k_z), \tag{32}$$

where $\varphi_{\mathbf{q}}$ is the angle between the vector potential and the z direction. The relevant term in the computation of transition probabilities is $|g_{\alpha\alpha',\mathbf{q}}|^2$, which contains a $\cos^2\varphi_{\mathbf{q}}$ term. If we consider a blackbody radiation we can assume it as composed of a superposition of plane waves with random polarization and thus we would replace $\cos^2\varphi_{\mathbf{q}}$ with its mean value over $(0,2\pi)$, that is, 1/2. Anyway each electromagnetic mode is the sum of two independent polarizations thus we may simply replace $\cos^2\varphi_{\mathbf{q}} \approx 1$, obtaining

$$g_{\alpha\alpha',\mathbf{q}} = \frac{\hbar e}{m\sqrt{2}} \delta(\mathbf{k}_{\alpha} - \mathbf{k}_{\alpha'}) |\mathbf{A}_{\mathbf{q}}| p_{\alpha\alpha'}, \tag{33}$$

where

$$p_{\alpha\alpha'} = \sum_{n} c^{*}_{b'nk'_z} c_{bnk_z} (G_n + k_z) \tag{34}$$

is the matrix element of the momentum operator between states α' and α.

Let us now consider a photon absorption process, bringing the system from state $|\alpha', n_{\mathbf{q}}\rangle$, with an electron in state α' and n photons with wavevector $\mathbf{q}$, to state $|\alpha, n_{\mathbf{q}}-1\rangle$, with the electron in state α and $(n-1)$ photons in state $\mathbf{q}$. Its probability per unit time can be evaluated by Fermi's golden rule as

$$P^{\text{opt}}_{\alpha\alpha',\mathbf{q}} = \frac{2\pi}{\hbar} |\langle \alpha, n_{\mathbf{q}} - 1 | \hat{H}^{\text{opt}} | \alpha', n_{\mathbf{q}} \rangle|^2 \delta(E_{\alpha} - E_{\alpha'} - \hbar\omega_{\mathbf{q}}). \tag{35}$$

The calculation gives

$$P^{\text{opt}}_{\alpha\alpha',\mathbf{q}} = \frac{2\pi}{\hbar} |g_{\alpha\alpha',\mathbf{q}}|^2 n_{\mathbf{q}} \delta(E_{\alpha} - E_{\alpha'} - \hbar\omega_{\mathbf{q}}). \tag{36}$$

On the other hand, the probability of a photon emission process, in which the system performs a transition from state $|\alpha, n_{\mathbf{q}}\rangle$ to state $|\alpha', n_{\mathbf{q}}+1\rangle$, is

$$P^{\text{opt}}_{\alpha'\alpha,\mathbf{q}} = \frac{2\pi}{\hbar} |g_{\alpha'\alpha,\mathbf{q}}|^2 (n_{\mathbf{q}} + 1) \delta(E_{\alpha} - E_{\alpha'} + \hbar\omega_{\mathbf{q}}). \tag{37}$$

F. Interaction with blackbody radiation

Since our aim is to determine the T_{blip} of our prototypical detector, we need to study its interaction with the background radiation, considered as a blackbody radiation at 300 K. From a quantum mechanical point of view, a blackbody radiation is a photon population at thermal equilibrium following the Bose–Einstein distribution law.

A noninteracting electron system only coupled to a photon bath at thermal equilibrium, must itself thermalize. Indeed, by employing the detailed-balance principle and substituting the Bose–Einstein distribution in Eqs. (36) and (37) we can write

$$\frac{f_{\alpha}}{f_{\alpha'}} = \frac{P^{\text{opt}}_{\alpha\alpha',\mathbf{q}}}{P^{\text{opt}}_{\alpha'\alpha,\mathbf{q}}} = \frac{n_{\mathbf{q}}}{(n_{\mathbf{q}}+1)} = e^{-\hbar\omega_{\mathbf{q}}/k_B T} = e^{-(E_{\alpha}-E_{\alpha'})/k_B T}, \tag{38}$$

that is, the steady-state distribution function is such that the ratio between the occupation numbers of states α and α' is, as expected, the Boltzmann factor.

Equations (36) and (37) give the transition probabilities for an electron interacting with an electromagnetic plane wave, which can be seen as an electromagnetic mode of a cavity. When our device is inside a cavity at thermal equilibrium (a blackbody), the total transition probabilities must be summed over all modes $\mathbf{q}$. This is also formally described by the interaction Hamiltonian (29), which is a sum over all wavevectors $\mathbf{q}$. We therefore write, for the absorption process,

$$P_{\alpha\alpha'}^{\text{opt}} = \sum_{\mathbf{q}} P_{\alpha\alpha',\mathbf{q}}^{\text{opt}} = \frac{2\pi}{\hbar} \sum_{\mathbf{q}} |g_{\alpha\alpha',\mathbf{q}}|^2 n_{\mathbf{q}} \delta(E_\alpha - E_{\alpha'} - \hbar\omega_{\mathbf{q}}). \tag{39}$$

In the limit of an infinitely large cavity, the summation becomes an integral in $d\mathbf{q}$ and $|g_{\alpha'\alpha,\mathbf{q}}|^2$ becomes a spectral density $|g_{\alpha'\alpha}(\mathbf{q})|^2$, which is related to the squared vector potential spectral density $|\mathcal{A}(\mathbf{q})|^2$ through Eq. (33).

The quantity $|\mathbf{A}(\mathbf{q})|^2$ can be expressed in terms of the energy density $U(\mathbf{q}) = \frac{1}{2}\varepsilon|\mathbf{E}(\mathbf{q})|^2 + 1/2\mu|\mathbf{B}(\mathbf{q})|^2$ and, considering the relations $\mathbf{E}(\mathbf{q}) = i\omega_{\mathbf{q}}\mathbf{A}(\mathbf{q})$ and $\mathbf{B} = \nabla \times \mathbf{A}$, as

$$|\mathbf{A}(\mathbf{q})|^2 = \frac{U(\mathbf{q})}{\varepsilon\omega_{\mathbf{q}}^2}. \tag{40}$$

For a linear dispersion relation $\omega_{\mathbf{q}} = cq$, we can switch from spectral densities in the wavevector domain to spectral densities in the frequency domain. In particular, we can consider the spectral energy density

$$U(\omega) = \frac{\hbar\omega^3}{4\pi^3 c^3}\mathcal{F}, \tag{41}$$

which is the energy density of an infinite cavity in which each mode is populated by one photon. The term $\mathcal{F}$ is a constant expressing the limited field-of-view (FOV) of the device and depending on how the blackbody radiation is coupled into the detector in the specific experimental setup. The absorption probability can then be evaluated in the frequency domain as

$$P_{\alpha\alpha'}^{\text{opt}} = \frac{2\pi}{\hbar^2} \int |g_{\alpha\alpha'}(\omega)|^2 n(\omega) \delta(\Delta\omega - \omega) d\omega$$

$$= \frac{2\pi}{\hbar^2} |g_{\alpha\alpha'}(\Delta\omega)|^2 n(\Delta\omega), \tag{42}$$

where $\Delta\omega = (E_\alpha - E_{\alpha'})/\hbar$ is the resonance frequency of the transition.

After substitution of Eqs. (33) and (40) into Eq. (42), we obtain

$$P_{\alpha\alpha'}^{\text{opt}} = U(\Delta\omega) \frac{\pi e^2}{m^2 \varepsilon \Delta\omega^2} |p_{\alpha\alpha'}|^2 n(\Delta\omega) \delta(\mathbf{k}_\alpha - \mathbf{k}_{\alpha'}). \tag{43}$$

Since we are dealing with a thermal population of photons we take $n(\Delta\omega)$ as the Bose–Einstein distribution function so that the total absorption probability can be finally written as

$$P_{\alpha\alpha'}^{\text{opt}} = \frac{e^2\hbar\Delta\omega\mathcal{F}}{4\pi^2 c^3 m^2 \varepsilon} |p_{\alpha\alpha'}|^2 \frac{1}{e^{\hbar\Delta\omega/k_B T} - 1} \delta(\mathbf{k}_\alpha - \mathbf{k}_{\alpha'}). \tag{44}$$

Analogously, the emission probability is

$$P_{\alpha'\alpha}^{\text{opt}} = \frac{e^2\hbar\Delta\omega\mathcal{F}}{4\pi^2 c^3 m^2 \varepsilon} |p_{\alpha'\alpha}|^2 \left[\frac{1}{e^{\hbar\Delta\omega/k_B T} - 1} + 1 \right] \delta(\mathbf{k}_{\alpha'} - \mathbf{k}_\alpha). \tag{45}$$

G. Fixing the value of τ

The model contains a free parameter τ, which has to be adjusted in order to reproduce some experimental data. Its value is, in principle, crucial in determining the T_{blip} of the simulated devices since changing the mean lifetime of electrons will change the strength of thermal scattering with respect to optical scattering and thus will affect the point at which these two competing processes balance.

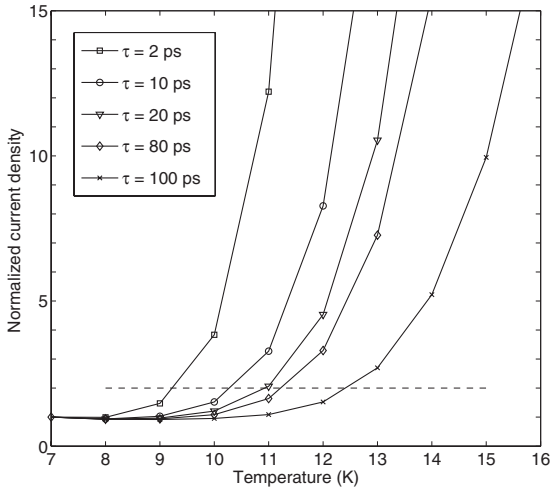

FIG. 2. Estimated normalized current density along the growth direction as a function of device temperature for the one-level QWIP in Fig. 1, operating at 3 THz in the presence of a background radiation field at 300 K. Different symbols correspond to different values of τ. The applied electric field is 50 V/cm, FOV is 90°. The dashed line marks the current doubling.

In particular, we choose to adjust τ in order to reproduce the measured T_{blip} (12 K) of the bound-to-continuum QWIP operating at 3.2 THz and reported in Ref. 21. Figure 2 shows the total normalized current densities that we obtain for a 3 THz QWIP as a function of temperature for different values of τ. Although τ is the key parameter that fixes the value of the T_{blip}, it can be noted from the figure that in the interval $\tau \approx 50-100$ ps, the T_{blip} shows little variation around 12 K. We can thus safely assume for τ any value in this range, such as, e.g., $\tau = 80$ ps, in order to reproduce the experimental data. It is important to stress once more, at this point, that this very large value derives from the fact that we are using a simplified model for thermal scattering; our fitting parameter τ is not to be taken as a realistic indication of electron scattering time in the real heterostructure. Once the value of τ has been set, on the basis of the above discussion, we use it in modeling the current response of detectors operating at identical frequencies but employing the proposed bound-to-bound-to-continuum strategy and differing in the number of bound states.

III. RESULTS AND DISCUSSION

We now apply the model of Sec. II to describe four different devices, having a number of bound levels ranging from one (standard QWIP) to four and designed according to our bound-to-bound-to-continuum strategy. All devices are exposed to a 300 K blackbody radiation under a 90° FOV and are subject to a 50 V/cm external bias.

Figure 3 shows the total normalized currents across each of the four devices as a function of the device temperature. Each curve allows one to identify a low-temperature regime in which the dark current is negligible with respect to the photocurrent: the total current is therefore independent from

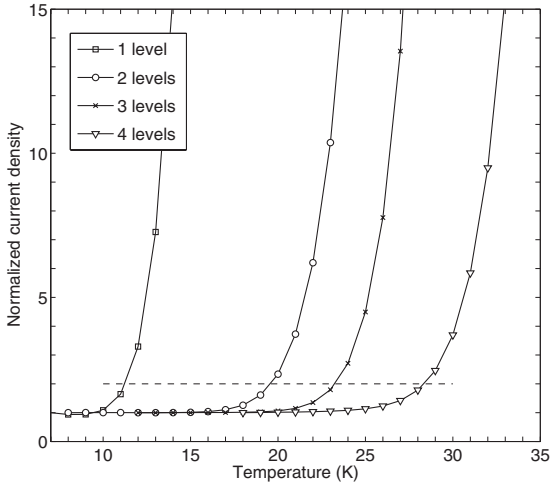

FIG. 3. Estimated current density (normalized) along the growth direction as a function of device temperature for the four diverse multilevel designs in Fig. 1 differing in the number of bound states.

the device temperature. Conversely, in the high temperature region, the dark current increases almost exponentially so that the photocurrent quickly becomes negligible and the current is totally due to the "dark" contribution. The T_{blip} may be identified as the temperature at which the total current doubles with respect to the low temperature region (dashed horizontal line in Fig. 3): at this temperature the dark current and the photocurrent have the same magnitude. The diverse designs have values of $T_{\mathrm{blip}}=11.5$, 19.5, 23.5, and 28.5 K for one, two, three, and four bound levels, respectively, showing the trend reported in Fig. 4.

The increase in T_{blip} may be better interpreted by looking at Fig. 5, where the photocurrent and the dark current are plotted as a function of the number of bound levels. Both currents decrease upon increasing the latter, but the dark current does it faster. Therefore, the temperature at which the two are equal moves toward higher values.

As can be observed in Fig. 5 there is a dramatic decrease in the photocurrent when switching from two to three bound states, which is mainly due to the reduction in the photoconductive gain. In fact, for the four-level design, the latter reduces to just the 0.2% of the value of the one-level QWIP. Conversely the quantum efficiency is only lowered by 14% and thus its variation does not significantly affect the photocurrent.

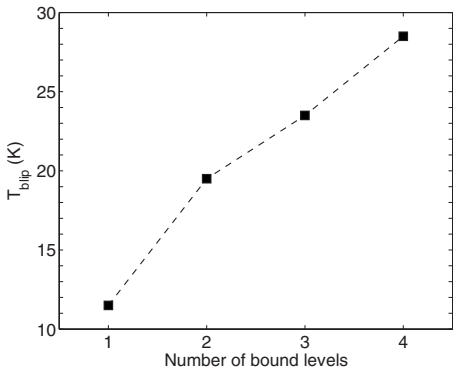

FIG. 4. Estimated values of T_{blip} for the four devices of Fig. 1, as deduced from the data shown in Fig. 3. The dashed line is a guide to the eyes.

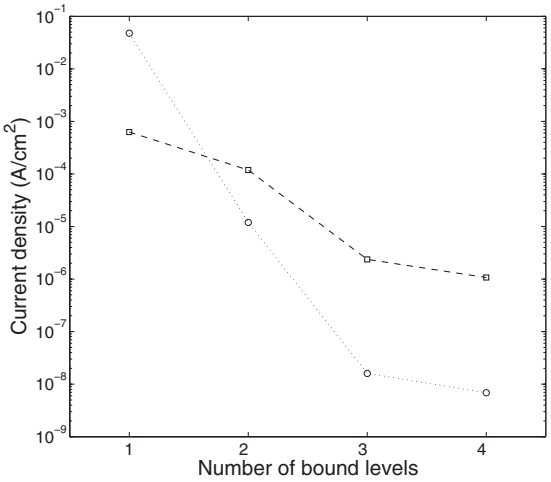

FIG. 5. Photocurrent (squares) and dark current at 17 K (circles) as a function of the number of levels in the device. The dark current decreases more rapidly than the photocurrent upon increasing the number of bound subbands, and thus the T_{blip} increases. Lines are guide to the eyes.

This behavior can be explained by considering Fig. 1 and noting that there is a remarkable geometrical difference between the two-level and the three-level designs. The presence of the nested QW introduces a new ground state whose wave function has little overlap with the wave functions of higher energy states, therefore reducing the oscillator strength. This conclusion is supported by the fact that the photocurrent reduction between the three and four levels designs, where no major structural change has been introduced, is comparable to the decrease between one and two level cases. In the present work the optimization of device performance is not the central issue; in this respect, a more elaborate tuning of the device geometry to achieve higher oscillator strengths would surely allow for better operational results.

IV. SUMMARY AND CONCLUSIONS

The scaling down of QWIPs to access the terahertz range of the electromagnetic spectrum is not straightforward: in this frequency range the dark current, mainly due to the high-energy tail of the electron distribution function, may indeed become predominant over the photocurrent signal. In a recent paper[22] we have proposed and theoretically investigated a terahertz-detector design alternative to the conventional QWIP structure. The former, instead of resorting on the conventional bound-to-continuum scheme, exploits a bound-to-bound-to-continuum strategy. In particular, a ladder of equally spaced bound levels is employed, whose energy step is tuned to the desired detection frequency.

Our previous analysis demonstrated that a multilevel architecture can indeed satisfactorily face the dark-current problem in far-infrared QWIPs. In the present paper we have significantly improved some features of our model to better reproduce the behavior of realistic state-of-the art designs. In particular, our attention has been devoted to a specific figure of merit of QWIPs, such as the background-limited infrared photodetection temperature (T_{blip}), which is related to the interplay between dark current and photocurrent. Our results

have demonstrated that the proposed multisubband scheme allows for higher T_{blip} values, with respect to conventional QWIP designs operating at the same frequency, and therefore could represent a better alternative for terahertz radiation detection.

APPENDIX A: POTENTIAL PROFILE CALCULATION

The key point of the proposed bound-to-bound-to-continuum architecture is the design of the nanostructure potential profile. The latter requires the solution of the inverse problem of setting the desired energy spectrum and then finding the corresponding operator, i.e., the potential energy term of the electron Hamiltonian H_e°. In the present paper, this problem has been solved numerically by means of a variational approach.

In particular, starting from the function $V(z)$ that describes the potential profile in one period of our device, a functional $\mathcal{F}[V(z)]$ has been defined whose value represents how far the function $V(z)$ is from our target function $\tilde{V}(z)$. The latter must be such that the operator

$$H = -\frac{\hbar^2}{2m}\frac{\partial^2}{\partial z^2} + \tilde{V}(z) \tag{A1}$$

has a spectrum composed of a lower part with $\tilde{N}$ equally spaced discrete values (bound states) and an upper continuous part. The number $\tilde{N}$ and the energy spacing $\tilde{E}$ of the bound states are our design constraints.

In general, a function $V(z)$ will produce N bound states of energies E_i, $i=1,\ldots,N$, where N can range from one to infinity (infinitely deep potential well). If there are two or more bound states we can define a mean interlevel spacing

$$E = \frac{1}{N}\sum_{i=1}^{N}(E_{i+1} - E_i) \tag{A2}$$

and a level spreading

$$\sigma = \frac{1}{N}\sum_{i=1}^{N}(E_i - E)^2. \tag{A3}$$

In terms of the quantities E and σ specified above, the functional $\mathcal{F}[V(z)]$ is defined as

$$\mathcal{F}[V(z)] = (1 - \delta_{N\tilde{N}}) + \sigma + |E - \tilde{E}|. \tag{A4}$$

From the latter equation we see that $\mathcal{F}$ is always positive and assumes the minimum, null, value only when $N=\tilde{N}$, $\sigma=0$, and $E=\tilde{E}$.

The actual existence of the minimum depends on the functional space we choose for $V(z)$. Indeed, we already know a solution for the problem $\mathcal{F}=0$, which is the harmonic oscillator, but the latter cannot be taken into consideration because it is not a realistic potential profile and its spectrum does not contain a continuous part.

Without going into the rigorous mathematical definition of the space, which is beyond the scope of the present paper, $V(z)$ must be a periodic function with period L_z. We therefore define $V(z)$ on the domain $-L_z/2 < z < L_z/2$ and impose $V(-L_z/2) = V(L_z/2)$. Of course we do not want $V(z)$ to diverge at any point and in addition we want it to be as close as possible to realistic and technologically accessible potential profiles.

We choose to take $V(z)$ piecewise constant on its domain so that it can be described by a discrete set of M parameters representing widths and depths of every constant sector. In this way, $V(z)$ can be represented by a point in an M-dimensional space and $\mathcal{F}$ actually becomes a function of M variables. In practice, $V(z)$ takes the form of a multi-quantum-well or a nested quantum-well structure, in which we vary depths and widths of the diverse layers.

The minimization of $\mathcal{F}$ is not trivial mainly because of the $\delta_{N\tilde{N}}$ term that makes it discontinuous in an unpredictable way: by slowly varying the free parameters, the potential profile can suddenly produce a new bound state or lose one causing $\mathcal{F}$ to jump by ± 1 and thus we cannot use methods that seek a local minimum following the function gradient.

We adopted the easiest possible solution: starting from an initial guess for $V(z)$, the free parameters are varied within a certain range to see if a minimum is present and whether the latter is actually the absolute one, for which $\mathcal{F}=0$. The existence of such minima mostly depends on the number M of free parameters that can be varied. We choose to start with the minimum number of parameters (which is two for a single quantum well) and then gradually increase this number in order to generate more bound states.

APPENDIX B: BOLTZMANN EQUATION SOLUTION

1. State space discretization

The electron dynamics in our prototypical quantum device is described by the Boltzmann transport equation (11). The latter will be solved by finite difference discretization of the derivatives and Reimann discretization of the integral.

Due to the cylindrical symmetry of the physical problem, guaranteed, as in our case, by an external field applied along the growth direction only, a convenient starting point is to employ cylindrical coordinates, with k_z being the perpendicular (growth direction) wavevector, and k_p and θ the modulus and anomaly, respectively, of the in-plane wavevector.

A central difference approximation of the derivatives along k_z may then be applied, with periodic boundary conditions accounting for the repetition of the Brillouin zone. In particular, the values of k_z span the first Brillouin zone $-\pi/L_Z < k_z < \pi/L_z$ forming a uniform grid of step N_{k_z}. The width of each discrete cell is therefore equal to $\Delta k_z = 2\pi/L_z N_{k_z}$.

The in-plane angle θ is uniformly discretized in the domain $[0, 2\pi)$. The number of discrete cells is N_θ and their size is $\Delta\theta = 2\pi/N_\theta$. Again, central difference approximation of derivatives and periodic boundary conditions are adopted.

Discretization along k_p poses the problem of limiting the in-plane $\mathbf{k}$-space. The electron distribution function $f(k_p)$ at thermal equilibrium has the form

$$f(k_p) \propto e^{-\hbar^2 k_p^2/2mk_BT} \tag{B1}$$

and thus decays rather quickly in k_p. We expect the electron nonequilibrium distribution to decay more or less in the same

way in the presence of the external radiation field. We therefore set a cutoff value f_{cut}, below which $f(k_p)$ is considered to be negligible, and use it to define a maximum value for k_p in the following way

$$k_p^{\max} = \sqrt{\frac{2mk_BT}{\hbar^2} \ln f_{\mathrm{cut}}}. \tag{B2}$$

The interval $[0, k_p^{\max}]$ is then discretized into a uniform grid of dimension N_{k_p}, and derivatives are approximated by central difference formulae in the inner nodes. In particular, $f(k_p=0)$ is supposed to have null derivative (Gaussian-like behavior) and the same applies for $f(k_p^{\max})$. Discrete cells along k_p have a width $\Delta k_p = k_p^{\max}/N_{k_p}$.

To complete the description of the state space we need to set the number N_b of subbands actually considered for calculations. The plane-wave solution of the Schrödinger equation requires from 1 to 200 plane waves to give stable energy level values, producing the same number of subbands. However, the electron distribution function decays rather quickly and a number of bands from five to a few tens are usually enough to ensure convergence. Indeed, the actual number of bands depends on the operating conditions of the device, such as the temperature and the presence of incident light or external bias.

2. Discrete Boltzmann equation

After discretization of the state space, the distribution function $f_b(\mathbf{k})$ can be itself discretized into a vector of components f_i. The label i ranges from 1 to the total number of grid points $N = N_{k_z} N_{k_p} N_\theta N_b$ and accounts for the band index b_i and the three $\mathbf{k}$-space coordinate indices $k_{z,i}$, $k_{p,i}$, and θ_i, collectively named $\mathbf{k}_i$. The value f_i is the mean of $f_{b_i}(\mathbf{k}_i)$ over the grid volume element $\Delta\mathbf{k}_i = \Delta k_{z,i} \Delta k_{p,i} \Delta\theta_i$

$$f_i = \frac{1}{\Delta\mathbf{k}_i} \int_{\Delta\mathbf{k}_i} f_{b_i}(\mathbf{k}_i) d\mathbf{k} \tag{B3}$$

from f_i we define the occupation number n_i of the ith discrete cell as

$$n_i = f_i \Delta\mathbf{k}_i. \tag{B4}$$

With this definition and taking into account relation (10) the occupation number is normalized as

$$\sum_i n_i = N_e. \tag{B5}$$

After the discretization of the distribution function, we need to find a suitable discretization of the scattering probabilities $P_{bb'}(\mathbf{k},\mathbf{k}')$. The total number of particles R_{ji} that perform a transition from the volume $\Delta\mathbf{k}_i$ in band b_i to the volume $\Delta\mathbf{k}_j$ in band b_j, is given by the probability that a particle in $\mathbf{k}_i$ performs a transition toward one of the states in volume $\Delta\mathbf{k}_j$, which is $\int_{\Delta\mathbf{k}_j} P_{b_j b_i}(\mathbf{k},\mathbf{k}_i) d\mathbf{k}$, integrated over all states of the starting volume

$$R_{ji} = \int_{\Delta\mathbf{k}_i} \int_{\Delta\mathbf{k}_j} f_{b_i}(\mathbf{k}') P_{b_j b_i}(\mathbf{k},\mathbf{k}') d\mathbf{k} d\mathbf{k}'. \tag{B6}$$

In the discretized system the probability that a particle performs the same transition is $P_{ji}\Delta\mathbf{k}_j$ and the number of particles in the starting volume is $n_i = f_i \Delta\mathbf{k}_i$, thus

$$R_{ji} = f_i \Delta\mathbf{k}_i P_{ji} \Delta\mathbf{k}_j. \tag{B7}$$

The combination of Eqs. (B6) and (B7) allow us to derive the following expression for P_{ji}:

$$P_{ji} = \frac{1}{f_i \Delta\mathbf{k}_i \Delta\mathbf{k}_j} \int_{\Delta\mathbf{k}_i} \int_{\Delta\mathbf{k}_j} f_{b_i}(\mathbf{k}') P_{b_j b_i}(\mathbf{k},\mathbf{k}') d\mathbf{k} d\mathbf{k}'. \tag{B8}$$

If we approximate $f_{b_i}(\mathbf{k}')$ with its mean value f_i over the volume $\Delta\mathbf{k}_i$, we can take it out of the integral and rewrite Eq. (B8) as

$$W_{ji} = P_{ji} \Delta\mathbf{k}_j = \frac{1}{\Delta\mathbf{k}_i} \int_{\Delta\mathbf{k}_i} \int_{\Delta\mathbf{k}_j} P_{b_j b_i}(\mathbf{k},\mathbf{k}') d\mathbf{k} d\mathbf{k}' \tag{B9}$$

and Eq. (B7) as

$$R_{ji} = W_{ji} n_i. \tag{B10}$$

The quantity W_{ji} is the probability that an event bringing an electron from a state i to one of the states in volume $\Delta\mathbf{k}_j$ occurs. By multiplying W_{ji} by the number of particles in the volume $\Delta\mathbf{k}_i$, that is, n_i, one obtains the rate R_{ji} of particles leaving the volume $\Delta\mathbf{k}_i$ and entering the volume $\Delta\mathbf{k}_j$.

For the generic ith volume element we can then write a rate equation in the usual form

$$\frac{\partial n_i}{\partial t} = \sum_j (W_{ij} n_j - W_{ji} n_i), \tag{B11}$$

which is the Boltzmann equation for a discrete system composed of N states. For the stationary state we write

$$\sum_j (W_{ij} n_j - W_{ji} n_i) = 0. \tag{B12}$$

Due to the discretization procedure, the drift term in Eq. (8) can be written as

$$\nabla f_b(\mathbf{k}) \cdot \frac{q}{\hbar}\mathbf{F} = \sum_j W_{ij}^D f_j, \tag{B13}$$

where W_{ij}^D is an equivalent scattering matrix that can be included into the W_{ij} term in Eq. (B12). The latter will in general consist of several contributions

$$W_{ij} = W_{ij}^D + W_{ij}^{\mathrm{th}} + W_{ij}^{\mathrm{opt}}, \tag{B14}$$

where W_{ij}^{th} and W_{ij}^{opt} are the discretized probability densities $P_{\alpha\alpha'}^{\mathrm{th}}$ and $P_{\alpha\alpha'}^{\mathrm{opt}}$, defined in Eqs. (18) and (44) and computed using Eq. (B9).

3. Nonoptical scattering probabilities

The derivation of Sec. II D can be followed in the discretized system by replacing $f_b(\mathbf{k})$ with f_i and $P_{bb'}(\mathbf{k},\mathbf{k}')$ with P_{ij}. In particular, the discretized version of Eq. (15)

$$\frac{1}{\tau} = \frac{1}{(2\pi)^3 N_e} \sum_{ij} P_{ji}^{\text{th}} \Delta\mathbf{k}_j \Delta\mathbf{k}_i \tag{B15}$$

leads to a definition of P_{ij}^{th} similar to Eq. (18)

$$P_{ij}^{\text{th}} = P_0 \mathcal{P}_{ij} = P_0 \begin{cases} 1 & \text{if } E_j > E_i \\ e^{-(E_i - E_j)/k_B T} & \text{if } E_j < E_i, \end{cases} \tag{B16}$$

where again P_0 is a normalization constant that can be computed as

$$\frac{1}{P_0} = \frac{\tau}{(2\pi)^3 N_e} \sum_{ij} \mathcal{P}_{ij} \Delta\mathbf{k}_j \Delta\mathbf{k}_i. \tag{B17}$$

The discrete thermal transition probabilities are then written according to Eq. (B9)

$$W_{ij}^{\text{th}} = P_{ij}^{\text{th}} \Delta\mathbf{k}_i. \tag{B18}$$

4. Optical scattering probabilities

The discrete optical scattering probabilities can be directly computed using Eqs. (B9) and (44) or Eq. (45). In both cases, the transition probabilities are of the form

$$P_{ij}^{\text{opt}}(\mathbf{k}_i, \mathbf{k}_j) = w_{ij} \delta(\mathbf{k}_i - \mathbf{k}_j), \tag{B19}$$

where w_{ij} contains all the coefficients and differs for absorption and emission processes. Substituting the latter expression into Eq. (B9) gives

$$W_{ij}^{\text{opt}} = \frac{1}{\Delta\mathbf{k}_j} \int_{\Delta\mathbf{k}_j} \int_{\Delta\mathbf{k}_i} w_{ij} \delta(\mathbf{k} - \mathbf{k}') d\mathbf{k}' d\mathbf{k}$$

$$= \frac{\delta_{ij}}{\Delta\mathbf{k}_j} \int_{\Delta\mathbf{k}_j} w_{ij} d\mathbf{k}. \tag{B20}$$

Assuming that w_{ij} is a smooth function over the volume cell $\Delta\mathbf{k}_j$ and for a sufficiently dense grid, we can approximate w_{ij} as a constant and take it out of the integral, which in turn results to be $\Delta\mathbf{k}_j$, therefore yielding

$$W_{ij}^{\text{opt}} = w_{ij} \delta_{ij}, \tag{B21}$$

which is the discrete transition probability to be used in the solution of the discrete Boltzmann equation.

[1] R. Köhler, A. Tredicucci, F. Beltram, H. E. Beere, E. H. Linfield, A. G. Davies, D. A. Ritchie, R. C. Iotti, and F. Rossi, Nature (London) **417**, 156 (2002).
[2] M. Rochat, L. Ajili, H. Willenberg, J. Faist, H. Beere, G. Davies, E. Linfield, and D. Ritchie, Appl. Phys. Lett. **81**, 1381 (2002).
[3] W. Knap, Y. Deng, S. Rumyantsev, J.-Q. Lü, M. S. Shur, C. A. Saylor, and L. C. Brunel, Appl. Phys. Lett. **80**, 3433 (2002).
[4] W. Knap, Y. Deng, S. Rumyantsev, and M. S. Shur, Appl. Phys. Lett. **81**, 4637 (2002).
[5] E. A. Shaner, M. Lee, M. C. Wanke, A. D. Grine, J. L. Reno, and S. J. Allen, Appl. Phys. Lett. **87**, 193507 (2005).
[6] C. Winnewisser, P. Uhd Jepsen, M. Shall, V. Schyja, and H. Helm, Appl. Phys. Lett. **70**, 3069 (1997).
[7] A. Nahata, J. T. Yardley, and T. F. Heinz, Appl. Phys. Lett. **75**, 2524 (1999).
[8] D. Hofstetter, M. Beck, and J. Faist, Appl. Phys. Lett. **81**, 2683 (2002).
[9] M. Graf, G. Scalari, D. Hofstetter, J. Faist, H. Beere, E. Linfield, D. Ritchie, and G. Davies, Appl. Phys. Lett. **84**, 475 (2004).
[10] *Intersubband Transitions in Quantum Wells: Physics and Device Applications I*, Semiconductors and Semimetals (Academic, San Diego, 2000), Vol. 62, Chap. 3, pp. 126–196.
[11] A. Majumdar, K. K. Choi, J. L. Reno, and D. C. Tsui, Appl. Phys. Lett. **83**, 5130 (2003).
[12] S. V. Bandara, S. Gunapala, J. K. Liu, S. B. Rafol, C. J. Hill, D. Z. Y. Ting, J. M. Fastenau, and A. W. K. Liu, Appl. Phys. Lett. **86**, 151104 (2005).
[13] M. P. Touse, G. Karunasiri, K. R. Lanz, H. Li, and T. Mei, Appl. Phys. Lett. **86**, 093501 (2005).
[14] J. Li, K. K. Choi, J. F. Klem, J. L. Reno, and D. C. Tsui, Appl. Phys. Lett. **89**, 081128 (2006).
[15] W. Liu, D. H. Zhang, Z. M. Huang, and W. J. Fan, J. Appl. Phys. **101**, 033114 (2007).
[16] H. C. Liu, E. Dupont, and M. Ershov, J. Nonlinear Opt. Phys. Mater. **83**, 5130 (2003).
[17] H. Schneider, T. Maier, H. C. Liu, M. Walther, and P. Koidl, Opt. Lett. **30**, 287 (2005).
[18] T. Maier, H. Schneider, M. Walther, P. Koidl, and H. C. Liu, Appl. Phys. Lett. **84**, 5162 (2004).
[19] T. Maier, H. Schneider, H. C. Liu, M. Walther, and P. Koidl, Appl. Phys. Lett. **88**, 051117 (2006).
[20] H. C. Liu, C. Y. Song, A. J. Spring Thorpe, and J. C. Cao, Appl. Phys. Lett. **84**, 4068 (2004).
[21] H. Luo, H. C. Liu, C. Y. Song, and Z. R. Wasilewski, Appl. Phys. Lett. **86**, 231103 (2005).
[22] F. Castellano, R. C. Iotti, and F. Rossi, Appl. Phys. Lett. **88**, 182111 (2006).
[23] F. Castellano, R. C. Iotti, and F. Rossi, Appl. Phys. Lett. **92**, 091108 (2008).
[24] S. Barbieri, F. Beltram, and F. Rossi, Phys. Rev. B **60**, 1953 (1999).